Experimental Realization of Nonadiabatic Holonomic Quantum Computation

Guanru Feng,[1,2] Guofu Xu,[1,2] and Guilu Long[1,2]

[1]State Key Laboratory of Low-Dimensional Quantum Physics and Department of Physics, Tsinghua University, Beijing 100084, China
[2]Tsinghua National Laboratory of Information Science and Technology, Beijing 100084, China

(Received 2 February 2013; revised manuscript received 7 March 2013; published 6 May 2013)

Because of its geometric nature, holonomic quantum computation is fault tolerant against certain types of control errors. Although proposed more than a decade ago, the experimental realization of holonomic quantum computation is still an open challenge. In this Letter, we report the first experimental demonstration of nonadiabatic holonomic quantum computation in a liquid NMR quantum information processor. Two noncommuting one-qubit holonomic gates, rotations about x and z axes, and the two-qubit holonomic CNOT gate are realized by evolving the work qubits and an ancillary qubit nonadiabatically. The successful realizations of these universal elementary gates in nonadiabatic holonomic quantum computation demonstrates the experimental feasibility of this quantum computing paradigm.

DOI: 10.1103/PhysRevLett.110.190501 PACS numbers: 03.67.Ac, 03.65.Vf, 03.67.Lx, 76.60.−k

Introduction.—Holonomic quantum computation (HQC) was first proposed by Zanardi and Rasetti [1]. In their original work, the twisting of eigenspaces of an adiabatically varying Hamiltonian was used to manipulate quantum states in a robust manner. Because of the geometric nature, HQC is robust against certain types of control errors. Since control errors are one main obstacle to the realization of quantum computation, HQC has become one promising quantum computation paradigm and has attracted increasing interests recently [2–18].

Early HQC is based on adiabatic evolution, in which states are encoded in degenerate eigenstates of a Hamiltonian, and gates are accomplished by adiabatically varying the Hamiltonian along a loop in the parameter space. Because of the adiabatic requirement, a long run time is naturally required in the parametric control in adiabatic HQC (AHQC). This not only limits the gate speed, but also exposes the system to an environment for a long time, and consequently leads to decoherence and reduces the efficiency of AHQC. To overcome these drawbacks in AHQC, nonadiabatic HQC (NHQC) has been pursued, and several NHQC protocols have been proposed [17,18]. In NHQC, the long run-time requirement is avoided, while still retaining all the robust advantages, making NHQC a very appealing quantum computing paradigm.

In this Letter, we report the first experimental realization of NHQC using a liquid NMR quantum information processor. The NHQC scheme we realize is based on a variant of the recently proposed NHQC scheme in Ref. [18]. In our modified NHQC scheme, decoherence-free subspace is not used and nonadiabatic holonomic evolution is achieved by nonadiabatically evolving the work qubits and an ancillary qubit. To experimentally realize universal quantum computation, nonadiabatic one-qubit holonomic rotation gates about x and z axes, and the nonadiabatic two-qubit holonomic CNOT gate are successfully implemented using a three-qubit NMR quantum information processor. These results demonstrate the experimental feasibility of NHQC.

Theoretical protocol.—We first briefly review the holonomic conditions. Consider an N-dimensional quantum system with its Hamiltonian $H(t)$. Assume the state of the system is initially in a M-dimensional subspace $\mathcal{S}(0)$ spanned by a set of orthonormal basis vectors $\{|\phi_k(0)\rangle\}_{k=1}^{M}$. It has been proven that [17,18] the evolution operator is a holonomic matrix acting on $\mathcal{S}(0)$ if $|\phi_k(t)\rangle$ satisfy the following conditions:

$$\text{(i)} \quad \sum_{k=1}^{M} |\phi_k(\tau)\rangle\langle\phi_k(\tau)| = \sum_{k=1}^{M} |\phi_k(0)\rangle\langle\phi_k(0)|, \tag{1}$$

$$\text{(ii)} \quad \langle\phi_k(t)|H(t)|\phi_l(t)\rangle = 0, k, l = 1, \ldots, M, \tag{2}$$

where τ is the evolution period and $|\phi_k(t)\rangle = \mathbf{T}\exp[-i\int_0^t H(t_1)dt_1]|\phi_k(0)\rangle$, with $\mathbf{T}$ being time ordering.

Now we construct the universal set of NHQC gates. For the nonadiabatic one-qubit holonomic rotation gates, a two-qubit system is used. We choose the logical qubit states as $|0\rangle_L = |10\rangle$, $|1\rangle_L = |11\rangle$. By such a design, all the information of the logical qubit is encoded in the work qubit (the second qubit), and the first qubit acts as an ancillary qubit. We design two types of Hamiltonians, $H_1(\phi_1)$ and $H_2(\phi_2)$, to respectively realize two noncommuting nonadiabatic one-qubit gates,

$$H_1(\phi_1) = \frac{1}{2}[a_1(X_1X_2 + Y_1Y_2) + b_1(X_1Y_2 - Y_1X_2) - a_1X_1(I_2 - Z_2) - b_1Y_1(I_2 - Z_2)], \tag{3}$$

$$H_2(\phi_2) = \frac{1}{2}[a_2(Y_1X_2 - X_1Y_2) - b_2X_1(I_2 - Z_2)], \tag{4}$$

where $a_1 = J_1\cos(\phi_1/2)$, $b_1 = J_1\sin(\phi_1/2)$, $a_2 = J_2\sin(\phi_2/2)$, $b_2 = J_2\cos(\phi_2/2)$, I is the one-qubit identity matrix, and X, Y, and Z are Pauli matrices. In the basis

$\{|00\rangle, |01\rangle, |10\rangle, |11\rangle\}$, the evolution operators $U_1^{\phi_1}(\tau_1)$ and $U_2^{\phi_2}(\tau_2)$ generated by $H_1(\phi_1)$ and $H_2(\phi_2)$, respectively, read

$$U_1^{\phi_1}(\tau_1) = \begin{pmatrix} 1 & 0 & 0 & 0 \\ 0 & -1 & 0 & 0 \\ 0 & 0 & 0 & e^{-i\phi_1} \\ 0 & 0 & e^{i\phi_1} & 0 \end{pmatrix}, \tag{5}$$

$$U_2^{\phi_2}(\tau_2) = \begin{pmatrix} 1 & 0 & 0 & 0 \\ 0 & -1 & 0 & 0 \\ 0 & 0 & \cos\phi_2 & i\sin\phi_2 \\ 0 & 0 & -i\sin\phi_2 & -\cos\phi_2 \end{pmatrix}, \tag{6}$$

where $J_1\tau_1 = \pi/\sqrt{2}$ and $J_2\tau_2 = \pi$. According to Eqs. (3)–(6), it is easy to prove that both conditions (i) and (ii) are satisfied if the state of the two-qubit system is initially in the logical subspace $S_1^L = \{|0\rangle_L, |1\rangle_L\}$. So $U_1^{\phi_1}(\tau_1)$ and $U_2^{\phi_2}(\tau_2)$ are holonomic matrices acting on S_1^L. In the basis $\{|0\rangle_L, |1\rangle_L\}$, $U_1^{\phi_1}(\tau_1)$ and $U_2^{\phi_2}(\tau_2)$ are, respectively, equivalent to

$$U_{xz}(\phi_1) = \begin{pmatrix} 0 & e^{-i\phi_1} \\ e^{i\phi_1} & 0 \end{pmatrix}, \tag{7}$$

$$U_{zx}(\phi_2) = \begin{pmatrix} \cos\phi_2 & i\sin\phi_2 \\ -i\sin\phi_2 & -\cos\phi_2 \end{pmatrix}. \tag{8}$$

Then the one-qubit holonomic rotation gates about x and z axes acting on the space S_1^L can be constructed by using U_{xz} and U_{zx},

$$R_z^L(\theta) = U_{xz}(0)U_{xz}\left(-\frac{\theta}{2}\right) \to U_1^0(\tau_1)U_1^{-(\theta/2)}(\tau_1), \tag{9}$$

$$R_x^L(\phi) = U_{zx}(0)U_{zx}\left(-\frac{\phi}{2}\right) \to U_2^0(\tau_2)U_2^{-(\phi/2)}(\tau_2). \tag{10}$$

From the above two gates, an arbitrary one-qubit NHQC operation can be built.

The nontrivial two-qubit NHQC gate we realize is the nonadiabatic holonomic CNOT gate. A three-qubit system is used to implement this gate. $|100\rangle$, $|101\rangle$, $|110\rangle$, and $|111\rangle$ are encoded as $|00\rangle_L$, $|01\rangle_L$, $|10\rangle_L$, and $|11\rangle_L$. We see that all the information of the logical two-qubit state is encoded in the two work qubits (the second qubit and the third qubit), and the first qubit acts as an ancillary qubit. The Hamiltonian H_3 for realizing the CNOT gate can be expressed as

$$H_3 = \frac{J_3}{4}[X_1(I_2 - Z_2)X_3 + Y_1(I_2 - Z_2)Y_3 - X_1(I_2 - Z_2)(I_3 - Z_3)]. \tag{11}$$

Letting the evolution time satisfy the condition $J_3\tau_3 = \pi/\sqrt{2}$, the evolution operator in the basis $\{|000\rangle, |001\rangle, |010\rangle, |011\rangle|100\rangle, |101\rangle, |110\rangle, |111\rangle\}$ reads

$$U_3(\tau_3) = \mathrm{Diag}[1, 1, 1, -1, 1, 1, X]. \tag{12}$$

According to Eqs. (11) and (12), we can prove that both conditions (i) and (ii) are satisfied if the state of the three-qubit system is initially in the logical subspace $S_2^L = \{|00\rangle_L, |01\rangle_L, |10\rangle_L, |11\rangle_L\}$. So $U_3(\tau_3)$ is a holonomic matrix acting on S_2^L. In the basis $\{|00\rangle_L, |01\rangle_L, |10\rangle_L, |11\rangle_L\}$, $U_3(\tau_3)$ is equivalent to the nonadiabatic holonomic CNOT gate.

As the Hamiltonians $H_1(\phi_1)$, $H_2(\phi_2)$, and H_3 are time independent, their holonomic evolution operators can be respectively written as

$$U_1^{\phi_1}(\tau_1) = \Pi_{l=1}^{N_1} U_1^{\phi_1}(\Delta t_1), \tag{13}$$

$$U_2^{\phi_2}(\tau_2) = \Pi_{l=1}^{N_2} U_2^{\phi_2}(\Delta t_2), \tag{14}$$

$$U_3(\tau_3) = \Pi_{l=1}^{N_3} U_3(\Delta t_3), \tag{15}$$

where Δt_i ($i \in \{1, 2, 3\}$) is small time interval and its value is τ_i/N_i, with N_i being the number of the time steps of the holonomic evolution. By using a modification of the Trotter formula which is correct up to $(\Delta t)^2$ [19], the short time evolutions respectively read

$$\begin{aligned} U_1^{\phi_1}(\Delta t_1) &= e^{-i\Delta t_1 H_1(\phi_1)} \approx T_1^{\phi_1}(\Delta t_1) \\ &= e^{i(\Delta t_1/2)*(b_1/2)Y_1(I_2-Z_2)} e^{i(\Delta t_1/2)*(a_1/2)X_1(I_2-Z_2)} e^{-i(\Delta t_1/2)*(b_1/2)(X_1Y_2-Y_1X_2)} e^{-i\Delta t_1*(a_1/2)(X_1X_2+Y_1Y_2)} \\ &\quad \times e^{-i(\Delta t_1/2)*(b_1/2)(X_1Y_2-Y_1X_2)} e^{i(\Delta t_1/2)*(a_1/2)X_1(I_2-Z_2)} e^{i(\Delta t_1/2)*(b_1/2)Y_1(I_2-Z_2)}, \end{aligned} \tag{16}$$

$$U_2^{\phi_2}(\Delta t_2) = e^{-i\Delta t_2 H_2(\phi_2)} \approx T_2^{\phi_2}(\Delta t_2) = e^{i(\Delta t_2/2)*(b_2/2)X_1(I_2-Z_2)} e^{-i\Delta t_2*(a_2/2)(Y_1X_2-X_1Y_2)} e^{i(\Delta t_2/2)*(b_2/2)X_1(I_2-Z_2)}, \tag{17}$$

$$\begin{aligned} U_3(\Delta t_3) &= e^{-i\Delta t_3 H_3} \approx T_3(\Delta t_3) \\ &= e^{i(\Delta t_3/2)*(J_3/4)X_1(I_2-Z_2)(I_3-Z_3)} e^{-i\Delta t_3*(J_3/4)X_1(I_2-Z_2)X_3} e^{-i\Delta t_3*(J_3/4)Y_1(I_2-Z_2)Y_3} e^{i(\Delta t_3/2)*(J_3/4)X_1(I_2-Z_2)(I_3-Z_3)}. \end{aligned} \tag{18}$$

Here $T_1^{\phi_1}(\Delta t_1)$, $T_2^{\phi_2}(\Delta t_2)$, and $T_3(\Delta t_3)$ can be realized by a combination of radio-frequency pulses and evolutions of the J-coupling constants between the neighboring qubits in the NMR technique [20–26]. According to Eqs. (13)–(18), the nonadiabatic holonomic gates $R_z^L(\theta)$, $R_x^L(\phi)$, and $U_{\rm cnot}^L$ can be realized by

$$R_z^L(\theta) \to \Pi_{l=1}^{N_1} T_1^0(\Delta t_1) \Pi_{l=1}^{N_1} T_1^{-(\theta/2)}(\Delta t_1), \tag{19}$$

$$R_x^L(\phi) \to U_2^0(\tau_2) \Pi_{l=1}^{N_2} T_2^{-(\phi/2)}(\Delta t_2), \tag{20}$$

$$U_{\rm cnot}^L \to \Pi_{l=1}^{N_3} T_3(\Delta t_3). \tag{21}$$

Notably, in Eq. (20), $U_2^0(\tau_2)$ can be implemented directly with no approximations; thus, it reads $U_2^0(\tau_2) = e^{i(\tau_2 J_2/2)(X_1 I_2 - X_1 Z_2)}$.

Experimental procedures and results.—Figures 1(a) and 1(b), respectively, illustrate the implementations of the nonadiabatic one-qubit and two-qubit holonomic gates. The diethyl-fluoromalonate dissolved in $d6$ acetone is used as the NMR quantum processor. ^{13}C, ^{19}F, and ^{1}H nuclear spins respectively act as the ancillary qubit and the two work qubits. Both in the one-qubit and two-qubit cases, the ancillary qubit stays in state $|1\rangle\langle 1|$ before and after the nonadiabatic holonomic evolutions. The input states (output states) of the work qubits are denoted as $\rho_{\rm in}^A$ ($\rho_{\rm out}^A$) and $\rho_{\rm in}^B$ ($\rho_{\rm out}^B$) for the one-qubit and two-qubit cases, respectively.

We here realize the following four one-qubit NHQC gates: $R_z^L(\pi/2)$, $R_z^L(\pi)$, $R_x^L(\pi/2)$, $R_x^L(\pi)$, and the NHQC CNOT gate $U_{\rm cnot}^L$. In order to demonstrate we can implement one-qubit NHQC gates on both ^{19}F and ^{1}H, $R_z^L(\pi/2)$ and $R_x^L(\pi/2)$ are implemented on ^{19}F and $R_z^L(\pi)$ and $R_x^L(\pi)$ are implemented on ^{1}H. In our experiments, the number of iterations is chosen to be $N_1 = 3$, $N_2 = 2$, and $N_3 = 2$. We prepare the initial states using the cat-state method [27–29]. For the one-qubit gates, we prepare the work qubit in $\rho_{\rm in}^A$ and the ancillary qubit in $|1\rangle\langle 1|$. Without loss of generality, the spectator work qubit is prepared in $|0\rangle\langle 0|$. Specifically, the NMR processor is initialized in the pseudopure states $|1\rangle\langle 1| \otimes \rho_{\rm in}^A \otimes |0\rangle\langle 0|$ [for $R_z^L(\pi/2)$ and $R_x^L(\pi/2)$] or $|1\rangle\langle 1| \otimes |0\rangle\langle 0| \otimes \rho_{\rm in}^A$ [for $R_z^L(\pi)$ and $R_x^L(\pi)$]. For the CNOT gate, the ancillary qubit is also prepared in $|1\rangle\langle 1|$ and the whole state of the NMR processor is $|1\rangle\langle 1| \otimes \rho_{\rm in}^B$. In terms of the deviation matrices [30], the input states $\rho_{\rm in}^A$ and $\rho_{\rm in}^B$ are prepared in each of the following sets:

$$\rho_{\rm in}^A \in \{X, Y, Z\}, \tag{22}$$

$$\rho_{\rm in}^B \in \{IX, IY, IZ, XI, XX, XY, XZ, YI, YX, YY, YZ, ZI, ZX, ZY, ZZ\}. \tag{23}$$

The output states $\rho_{\rm out}^A$ and $\rho_{\rm out}^B$ are determined by quantum state tomography [31]. To measure the sameness of the theoretical output state $\rho_{\rm th}$ and the experimental output state $\rho_{\rm out}$, the attenuated and unattenuated state fidelities [32,33], which are respectively defined as $\mathrm{Tr}(\rho_{\rm out}\rho_{\rm th})/\sqrt{\mathrm{Tr}(\rho_{\rm th}\rho_{\rm th})\mathrm{Tr}(\rho_{\rm in}\rho_{\rm in})}$ and $\mathrm{Tr}(\rho_{\rm out}\rho_{\rm th})/\sqrt{\mathrm{Tr}(\rho_{\rm out}\rho_{\rm out})\mathrm{Tr}(\rho_{\rm th}\rho_{\rm th})}$, are used. The attenuated fidelity takes into account the signal loss, while the unattenuated fidelity ignores certain errors due to the signal loss and quantifies how similar in direction $\rho_{\rm out}$ and $\rho_{\rm th}$ are [32,33]. The average experimental attenuated fidelities are 60.7%, 61.8%, 86.1%, 77.7%, and 47.9% for the output states of $R_z^L(\pi/2)$, $R_z^L(\pi)$, $R_x^L(\pi/2)$, $R_x^L(\pi)$, and $U_{\rm cnot}^L$, respectively, while their average experimental unattenuated fidelities are 97.6%, 97.3%, 97.9%, 95.7%, and 93.12%, respectively. These numbers are in line with the results of other experiments done using diethyl-fluoromalonate [34]. The differences between the attenuated and unattenuated fidelities are consistent with the signal loss rates measured in our experiments (see Supplemental Material [35]). Figure 2 shows the unattenuated output state fidelities in our experiments. Figure 3 shows example NMR experimental spectra. Figure 3(a) [Fig. 3(d)] is the ^{13}C spectrum of the input state $\rho_{\rm in}^A = X$ for ^{1}H (^{19}F), with ^{19}F (^{1}H) in state $|0\rangle\langle 0|$. Figures 3(b), 3(c), 3(e), and 3(f) show the ^{13}C spectra of the output states $\rho_{\rm out}^A$, after implementing $R_x^L(\pi)$, $R_z^L(\pi)$, $R_x^L(\pi/2)$, and $R_z^L(\pi/2)$ to the input states $\rho_{\rm in}^A = X$, respectively. Figures 3(g) and 3(h) show the spectra of $\rho_{\rm in}^B = IX$ and $\rho_{\rm out}^B$ after applying $U_{\rm cnot}^L$.

Quantum process tomography (QPT) [36] is used to quantitatively describe the implementation of the NHQC gates. According to QPT, each quantum process is characterized by a χ matrix. For a given input state $\rho_{\rm in}$, the output state is expressed as $\rho_{\rm out} = \Sigma_{k,l}\chi_{kl} e_k \rho_{in} e_l^\dagger$, where e_k

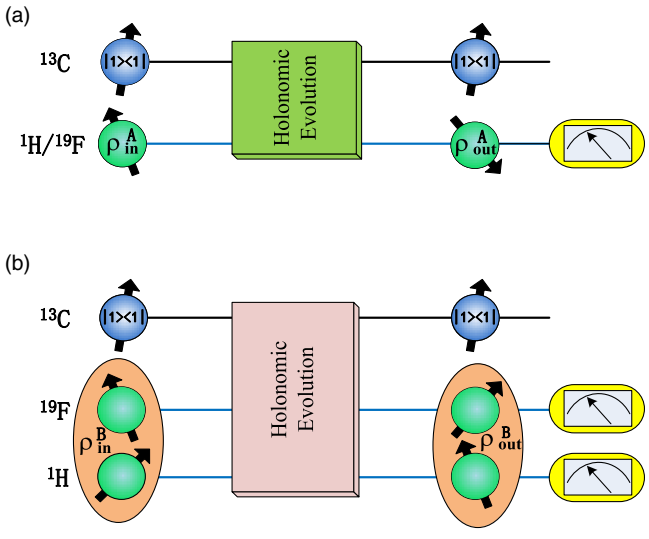

FIG. 1 (color online). Circuits for the NHQC gates. (a) The one-qubit NHQC gates. (b) The two-qubit NHQC gate. In both (a) and (b), ^{13}C acts as an ancillary qubit and stays in state $|1\rangle\langle 1|$ before and after the nonadiabatic holonomic evolutions. ^{19}F and ^{1}H nuclear spins are the two work qubits.

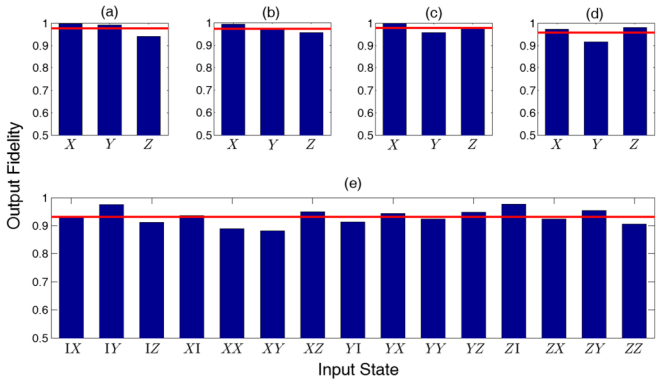

FIG. 2 (color online). The experimental unattenuated output state fidelities for the NHQC gates. In (a), (b), (c), and (d) are the fidelities of ρ^A_{out} for $R^L_z(\pi/2)$, $R^L_z(\pi)$, $R^L_x(\pi/2)$, and $R^L_x(\pi)$ respectively, applied to input states X, Y, and Z. $R^L_z(\pi/2)$ and $R^L_x(\pi/2)$ are implemented on ^{19}F; $R^L_z(\pi)$ and $R^L_x(\pi)$ are implemented on ^{1}H. In (e) are the fidelities of ρ^B_{out} for U^L_{cnot}, applied to 15 different input states listed in Eq. (23). The average fidelities (the red solid horizontal lines) are 97.6%, 97.3%, 97.9%, 95.7%, and 93.12% in (a)—(e), respectively.

belongs to an operation basis set. The elements of the operator basis set for the one-qubit and two-qubit cases can be, respectively, chosen as

$$e_k \in \{I, X, -iY, Z\}, k = 1, ..., 4, \tag{24}$$

$$e_k \in \{II, IX, -iIY, IZ, XI, XX, -iXY, XZ, -iYI, -iYX, -YY, -iYZ, ZI, ZX, -iZY, ZZ\}, k = 1, \ldots, 16. \tag{25}$$

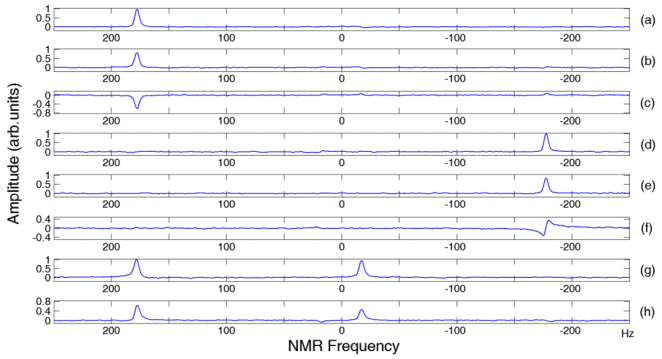

FIG. 3 (color online). Experimental spectra of ^{13}C. (a) and (d) are, respectively, the spectra obtained by observing the states with ^{1}H and ^{19}F in $\rho^A_{\text{in}} = X$, with no holonomic operations. (b), (c), (e), and (f) are the spectra of ρ^A_{out}, starting with the initial states $\rho^A_{\text{in}} = X$, and applying the holonomic operations $R^L_x(\pi)$, $R^L_z(\pi)$, $R^L_x(\pi/2)$, and $R^L_z(\pi/2)$, respectively. $R^L_x(\pi)$ and $R^L_z(\pi)$ are implemented on ^{1}H; $R^L_x(\pi/2)$ and $R^L_z(\pi/2)$ are implemented on ^{19}F. (g) is the spectrum of the initial state $\rho^B_{\text{in}} = IX$. (h) is the spectrum of ρ^B_{out} after the holonomic operation U^L_{cnot} with the initial state $\rho^B_{\text{in}} = IX$. (a), (d), and (g) are used as reference spectra, to which (b), (c), (e), (f), and (h) are normalized. All the observation is realized by transferring the states of the work qubits to ^{13}C and then observing ^{13}C.

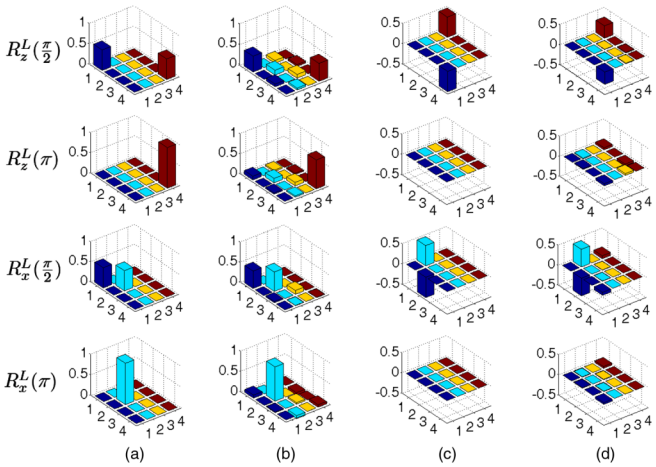

FIG. 4 (color online). The QPT χ matrices of one-qubit holonomic gates $R^L_z(\pi/2)$, $R^L_z(\pi)$, $R^L_x(\pi/2)$, and $R^L_x(\pi)$. The (a) and (c) columns are the real parts and imaginary parts of the theoretical χ matrices, respectively. The (b) and (d) columns are the real parts and imaginary parts of the experimental χ matrices, respectively. The numbers in the x and y axes refer to the operators in the operator basis set $\{I, X, -iY, Z\}$.

The QPT χ matrix is calculated using the output states via the technique described in Ref. [19]. The experimental χ for one-qubit and two-qubit gates is shown in Figs. 4 and 5, respectively. We use χ fidelities to evaluate the performance of NHQC gates. The attenuated χ fidelities $|\text{Tr}(\chi_{\text{exp}}\chi^\dagger_{\text{th}})|$ [33], which take into account the signal loss, are 70.5%, 71.3%, 89.5%, 83.3%, and 51.2% for the $R^L_z(\pi/2)$, $R^L_z(\pi)$, $R^L_x(\pi/2)$, $R^L_x(\pi)$, and U^L_{cnot} gates, respectively. The deviations between χ_{th} and χ_{exp} are mainly

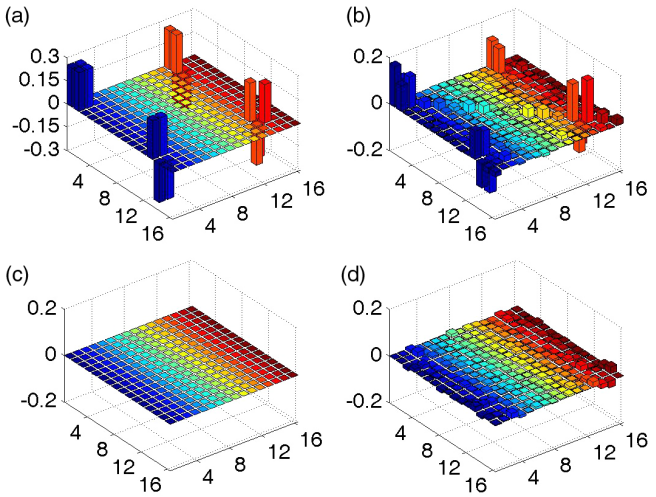

FIG. 5 (color online). The QPT χ matrices of U^L_{cnot}. (a) and (c) are the real part and imaginary part of the theoretical χ matrix, respectively. (b) and (d) are the real part and imaginary part of the experimental χ matrix, respectively. The numbers 1 to 16 in the x and y axes refer to the operators in the operator basis set $\{II, IX, -iIY, IZ, XI, XX, -iXY, XZ, -iYI, -iYX, -YY, -iYZ, ZI, ZX, -iZY, ZZ\}$.

caused by an overall loss of signal. To see the sameness of theoretical and experimental quantum processes when ignoring certain errors due to signal loss, we use the unattenuated χ fidelity defined as $|\mathrm{Tr}(\chi_{\mathrm{exp}}\chi_{\mathrm{th}}^{\dagger})|/\sqrt{\mathrm{Tr}(\chi_{\mathrm{exp}}\chi_{\mathrm{exp}}^{\dagger})\mathrm{Tr}(\chi_{\mathrm{th}}\chi_{\mathrm{th}}^{\dagger})}$ [33,37,38]. The unattenuated experimental χ fidelities of the gates $R_z^L(\pi/2)$, $R_z^L(\pi)$, $R_x^L(\pi/2)$, $R_x^L(\pi)$, and U_{cnot}^L are 95.9%, 95.9%, 98.1%, 96.3%, and 91.43%, respectively. It is interesting to note that the Trotter approximations in Eqs. (16)–(18) give very good approximations to the exact evolution and the theoretical χ fidelities are 99.2%, 98.6%, 99.2%, 97.4%, and 98.7% for $R_z^L(\pi/2)$, $R_z^L(\pi)$, $R_x^L(\pi/2)$, $R_x^L(\pi)$, and U_{cnot}^L, respectively.

Summary.—As a proof of principle, we experimentally implemented NHQC via a NMR quantum information processor using a variant version of the scheme proposed in Ref. [18]. In our experiments, one-qubit nonadiabatic holonomic gates and two-qubit holonomic CNOT gates, which compose a universal set of NHQC gates, are implemented by using an ancillary qubit which provides the additional dimension needed in the holonomic evolution. This is the first experimental demonstration of NHQC, which is a step toward fault-tolerant quantum computing. The successful realizations of these universal elementary gates in NHQC demonstrate the feasibility of implementing NHQC using present experimental techniques.

This work is supported by the National Natural Science Foundation of China (Grants No. 11175094 and No. 91221205), and the National Basic Research Program of China (2009CB929402, 2011CB9216002). The authors also thank IQC, University of Waterloo, for providing the NMR software compiler.

[1] P. Zanardi and M. Rasetti, Phys. Lett. A **264**, 94 (1999).
[2] J. A. Jones, V. Vedral, A. Ekert, and G. Castagnoli, Nature (London) **403**, 869 (2000).
[3] G. Falci, R. Fazio, G. Massimo Palma, J. Siewert, and V. Vedral, Nature (London) **407**, 355 (2000).
[4] L. M. Duan, J. I. Cirac, and P. Zoller, Science **292**, 1695 (2001).
[5] S. L. Zhu and Z. D. Wang, Phys. Rev. Lett. **91**, 187902 (2003).
[6] L.-A. Wu, P. Zanardi, and D. A. Lidar, Phys. Rev. Lett. **95**, 130501 (2005).
[7] L. X. Cen, Z. D. Wang, and S. J. Wang, Phys. Rev. A **74**, 032321 (2006).
[8] X. D. Zhang, Q. H. Zhang, and Z. D. Wang, Phys. Rev. A **74**, 034302 (2006).
[9] P. J. Leek, J. M. Fink, A. Blais, R. Bianchetti, M. Goppl, J. M. Gambetta, D. I. Schuster, L. Frunzio, R. J. Schoelkopf, and A. Wallraff, Science **318**, 1889 (2007).
[10] M. Möttönen, J. J. Vartiainen, and J. P. Pekola, Phys. Rev. Lett. **100**, 177201 (2008).
[11] X. L. Feng, C. F. Wu, H. Sun, and C. H. Oh, Phys. Rev. Lett. **103**, 200501 (2009).
[12] O. Oreshkov, T. A. Brun, and D. A. Lidar, Phys. Rev. Lett. **102**, 070502 (2009).
[13] V. N. Golovach, M. Borhani, and D. Loss, Phys. Rev. A **81**, 022315 (2010).
[14] J. T. Thomas, M. Lababidi, and M. Z. Tian, Phys. Rev. A **84**, 042335 (2011).
[15] X.-B. Wang, and M. Keiji, Phys. Rev. Lett. **87**, 097901 (2001).
[16] M. Pechal, S. Berger, A. A. Abdumalikov, J. M. Fink, J. A. Mlynek, L. Steffen, A. Wallraff, and S. Filipp, Phys. Rev. Lett. **108**, 170401 (2012).
[17] E. Sjöqvist, D. M. Tong, B. Hessmo, M. Johansson, and K. Singh, New J. Phys. **14**, 103035 (2012).
[18] G. F. Xu, J. Zhang, D. M. Tong, E. Sjöqvist, and L. C. Kwek, Phys. Rev. Lett. **109**, 170501 (2012).
[19] M. Nielsen and I. Chuang, *Quantum Computation and Quantum Information* (Cambridge University Press, Cambridge, 2000).
[20] L. M. K. Vandersypen and I. L. Chuang, Rev. Mod. Phys. **76**, 1037 (2005).
[21] X.-H. Peng, J.-F. Du, and D. Suter, Phys. Rev. A **71**, 012307 (2005).
[22] R. Somma, G. Ortiz, J. E. Gubernatis, E. Knill, and R. Laflamme, Phys. Rev. A **65**, 042323 (2002).
[23] A. Barenco, C. H. Bennett, R. Cleve, D. P. DiVincenzo, N. Margolus, P. Shor, T. Sleator, J. A. Smolin, and H. Weinfurter, Phys. Rev. A **52**, 3457 (1995).
[24] L. M. K. Vandersypen, M. Steffen, M. H. Sherwood, C. S. Yannoni, G. Breyta, and I. L. Chuang, Appl. Phys. Lett. **76**, 646 (2000).
[25] C. H. Tseng, S. Somaroo, Y. Sharf, E. Knill, R. Laflamme, T. F. Havel, and D. G. Cory, Phys. Rev. A **61**, 012302 (1999).
[26] C. A. Ryan, C. Negrevergne, M. Laforest, E. Knill, and R. Laflamme, Phys. Rev. A **78**, 012328 (2008).
[27] E. Knill, R. Laflamme, R. Martinez, and C.-H. Tseng, Nature (London) **404**, 368 (2000).
[28] A. M. Souza, J.-F. Zhang, C. A. Ryan, and R. Laflamme, Nat. Commun. **2**, 169 (2011).
[29] J.-F. Zhang, M.-H. Yung, R. Laflamme, A. Aspuru-Guzik, and J. Baugh, Nat. Commun. **3**, 880 (2012).
[30] I. L. Chuang, N. Gershenfeld, M. G. Kubinec, and D. W. Leung, Proc. R. Soc. A **454**, 447 (1998).
[31] J.-S. Lee, Phys. Lett. A **305**, 349 (2002).
[32] E. M. Fortunato, M. A. Pravia, N. Boulant, G. Teklemariam, T. F. Havel, and D. G. Cory, J. Chem. Phys. **116**, 7599 (2002).
[33] Y. S. Weinstein, T. F. Havel, J. Emerson, N. Boulant, M. Saraceno, S. Lloyd, and D. G. Cory, J. Chem. Phys. **121**, 6117 (2004).
[34] X.-H. Peng, J.-F. Zhang, J.-F. Du, and D. Suter, Phys. Rev. Lett. **103**, 140501 (2009).
[35] See Supplemental Material at http://link.aps.org/supplemental/10.1103/PhysRevLett.110.190501 for the signal loss rates listed in Section 6.
[36] I. L. Chuang and M. A. Nielsen, J. Mod. Opt. **44**, 2455 (1997); J. F. Poyatos, J. I. Cirac, and P. Zoller, Phys. Rev. Lett. **78**, 390 (1997).
[37] X. Wang, C.-S. Yu, and X. X. Yi, Phys. Lett. A **373**, 58 (2008).
[38] J.-F. Zhang, R. Laflamme, and D. Suter, Phys. Rev. Lett. **109**, 100503 (2012).